Infrared-laser-induced upconversion from Nd^{3+}:LaF$_3$ heteroepitaxial layers on CaF$_2$(111) substrates by molecular beam epitaxy

X. Zhang,[1,2,*] C. Serrano,[1] E. Daran,[1] F. Lahoz,[1,3] G. Lacoste,[1] and A. Muñoz-Yagüe[1]

[1]*Laboratoire d'Analyse et d'Architecture des Système du CNRS, 7, Avenue du Colonel Roche, 31077 Toulouse cedex 4, France*

[2]*Photonics Research Group, Division of Microelectronics, School of Electrical and Electronic Engineering, Nanyang Technological University, Nanyang Avenue, Singapore 639798*

[3]*ICMA, Universidad de Zaragoza—CSIC, Pza. San Francisco s/n, 50009 Zaragoza, Spain*

This paper reports a systematic analysis on the upconversion fluorescence from a Nd^{3+}-doped LaF$_3$ planar waveguide grown on (111) oriented CaF$_2$ substrates by molecular beam epitaxy. A spectroscopic study of upconversion emission has been carried out at low temperature. Upon infrared excitation into the $^2H_{9/2}$, $^4F_{5/2}$, or $^4F_{3/2}$ multiplets of Nd^{3+}, strong uv upconversion emissions originating from $^4D_{3/2}$ to ^4I_J ($J = \frac{9}{2}$, $\frac{11}{2}$, and $\frac{13}{2}$) transitions by a three-photon process have been observed. In addition, other upconversion emissions in the green and orange regions due to two-photon processes were also obtained and attributed to the $^4G_{7/2} \rightarrow {}^4I_{9/2}$, $^2G_{7/2} + {}^4G_{5/2} \rightarrow {}^4I_{9/2}$, and $^4G_{7/2} \rightarrow {}^4I_{11/2}$ transitions, respectively. In accordance with our experimental results, two kinds of energy-transfer processes are proposed as upconversion mechanisms responsible for the different emissions, and which are supported by a rate-equation analysis. The green and orange upconversions originate from an energy-transfer process involving two Nd^{3+} ions excited in the $^4F_{3/2}$ state. For the three-photon upconversion, two successive energy cross-relaxation are suggested to populate the $^4D_{3/2}$ level. The concentration dependence study has shown that the optimum concentration for a Nd^{3+} dopant is about 1 at. % for all the upconversion emissions. Owing to a guided configuration, upconversion emissions that are hardly detectable in a nonguided configuration at temperature higher than 100 K have now been recorded at room temperature.

I. INTRODUCTION

Short-wavelength solid-state lasers in the uv to green spectral range have attracted much attention in recent years due to a wide range of applications including optical data storage, color display, infrared sensor, and so on. Several approaches have been made on the II-VI and III-V groups' wide-band semiconductor diode lasers, the frequency doubling by using nonlinear crystals, the optical parametric oscillator, and the phenomenon of frequency upconversion by using the intrinsic energy-level matching of certain rare-earth ions. In upconversion processes, an emission photon with a wavelength shorter than that of an excitation photon is obtained as a result of multiphoton processes involving two or more excitation photons. The phenomena and mechanisms of upconversion fluorescence have been studied for rare-earth ions in various hosts during the past two decades.[1–5] Upconversion laser action has been demonstrated from rare-earth ions such as Er^{3+}, Tm^{3+}, Ho^{3+}, Nd^{3+}, and Pr^{3+} both at low and room temperatures.[6]

Nd^{3+} has been recognized as one of the most efficient rare-earth ions for solid-state lasers in various materials[7] due to its intense emission at 1.06 μm. Recent spectroscopic results showed that the Nd^{3+} ion could be also used as a good candidate for upconversion fluorescence and lasers.[8–10] Upconversion fluorescence from Nd^{3+} in LaF$_3$ bulk crystals has been studied before.[11–13] Green or blue laser operations with Nd^{3+} upon infrared laser excitation have been realized in LaF$_3$ (Ref. 14) and YLiF$_4$ (Ref. 15) monocrystals at low temperature ($<$90 K) and in ZBLAN glass[16] at room tem-

perature (RT). In order to find high luminescence efficiency and RT laser operation, a great deal of materials doped with Nd^{3+} has been examined comprising both crystals and glasses.[6,10,17,18] Russel *et al.* have recently reported their systematic upconversion study on Nd^{3+}-doped KLiYF$_5$ crystal at high pump density supplied by a Ti:sapphire laser between 785 and 811 nm.[17] They have shown that efficient blue and green upconversion can be obtained at RT by energy-transfer processes. Room-temperature uv upconversion with 866-nm pumping for Nd^{3+} activated fluoroindate glass has been reported by Menezes *et al.*[18]

Materials with a waveguide structure including planar or channel waveguides and optical glass fiber have shown more potentiality in obtaining high-temperature upconversion emission and laser operation compared to that of bulk materials, due to the high confinement of excitation radiation in these guided configurations. In this respect, molecular beam epitaxy (MBE) has shown many advantages in elaborating the rare-earth ion-doped thin film waveguide, such as the uniformity of the crystalline layer and the relatively low growth temperature. Furthermore, an accurate control of thickness, composition, and doping concentrations, the ability to make controlled composition changes, and growth of multilayer stacks could facilitate in optimizing waveguide structures. Upconversion studies for this kind of layer have been reported in Er^{3+}-doped CaF$_2$,[19] ZnF$_2$,[20] and LaF$_3$ (Ref. 21) crystalline layers. In a U.S. patent, MacFarlane *et al.* have described an upconversion device for visible laser operation by using Er^{3+}-doped fluoride crystalline planar and channel waveguides.[22]

Recently, we have demonstrated the first laser operation in Nd^{3+}-doped fluoride waveguide elaborated by MBE. Laser emission at 1.06 μm was obtained from Nd^{3+}-doped LaF_3 heteroepitaxial layers on (111) oriented CaF_2 substrates with an excitation threshold lower than 70 mW.[23] In this paper, we report the infrared to uv and green upconversions from these epitaxial layers. Three- and two-photon upconversion emissions from $^4D_{3/2}$ and $^4G_{7/2}$, $(^2G_{7/2}+^4G_{5/2})$ levels, respectively, have been observed at low temperature. With a waveguided configuration, an RT upconversion has been recorded at blue, green, and orange wavelength ranges for these epitaxial layers by using a prism-coupling technique.

II. EXPERIMENT

The Nd^{3+}-doped LaF_3 crystalline layers were grown by the molecular beam epitaxy technique.[24] 1-mm-thick CaF_2 crystals with a (111) oriented face were used as substrates for the epitaxial growth. We chose the (111) oriented CaF_2 as a substrate because crystal growth of LaF_3 layers on this direction has the lowest lattice mismatch with a CaF_2 substrate that should result in the optimum optical quality of the epitaxial layers. Two separate effusion cells of LaF_3 and NdF_3 were used in order to facilitate the control of Nd^{3+}-doping concentration. Epitaxial growth was performed under an ultrahigh vacuum ($<10^{-9}$ torr) to ensure a low contamination level of undesirable species, such as oxygen. The growth temperature for the substrate is 520 °C and the effusion cell temperatures were controlled to obtain a typical growth rate of 0.7 μm/h and a doping concentration of Nd^{3+} ranging from 0 to 5 at. %.

Upconversion measurements for the epitaxial layers were performed by using a cw tunable Ti:sapphire laser. The samples were fixed in a cryostat circulated by liquid helium to obtain a working temperature ranging from 25 K to RT. The excitation radiation was focused onto the active layer by a lens with a focal length of 8 cm and a prism is used to reflect the excitation source in a backreflecting configuration. A luminescence signal collected by two lenses with a 16-cm focal length was dispersed by a 1-m Jobin-Yvon monochromator and detected by a GaAs photodiode (PM 636), then amplified by a lock-in amplifier. For the fluorescence dynamic measurements, a digital oscilloscope with a time resolution of 5 ns (Model Philips PM/3323) was used to record the decay and rise signals. The recorded data were then analyzed by a computer to fit the time constants.

The refractive indices for the waveguide layers and the substrate crystals, as well as the RT upconversion properties have been characterized using a prism-coupling technique. For the index measurements, a convergent light was used, while for the upconversion study, a parallel light was used to excite only one guided mode. The feature of the excitation light was ensured by a series of optical lenses and a pinhole.

III. RESULTS

A. Low-temperature spectroscopy

Upon infrared radiation from a Ti:sapphire laser, upconversion emissions of Nd^{3+}-doped LaF_3 layers were detected at about 25 K, mainly in three regions: between 350 and 420
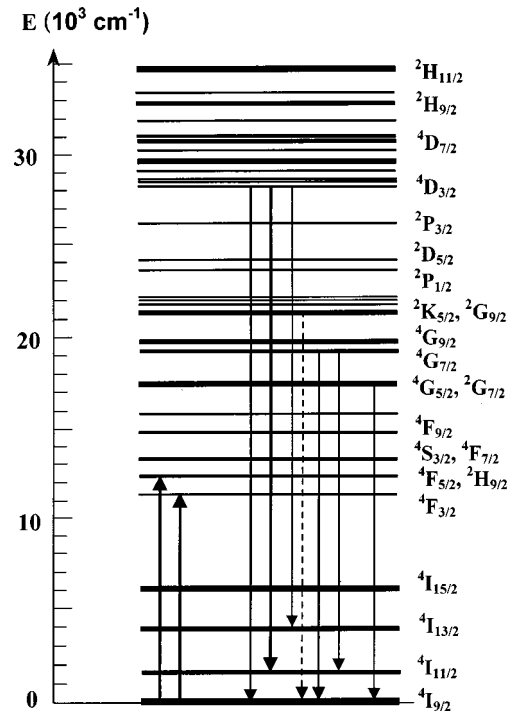

FIG. 1. Energy levels of the Nd^{3+} ion in LaF_3 crystal. The upconversion emissions observed in this work and the pump levels are indicated. Dashed line indicates the upconversion only observed under guided excitation at RT.

nm due to the transitions of $^4D_{3/2}\rightarrow^4I_J$ ($J=\frac{9}{2}$, $\frac{11}{2}$, and $\frac{13}{2}$); from 510 to 540 nm due to the $^4G_{7/2}\rightarrow^4I_{9/2}$ transition; and from 570 to 600 nm resulting from two transitions of $^4G_{7/2}\rightarrow^4I_{11/2}$ and $^2G_{7/2}+^4G_{5/2}\rightarrow^4I_{9/2}$. In order to facilitate the explanation thereafter, the energy-level diagram of Nd^{3+} in LaF_3 bulk crystal established by Canall et al.[25] is shown in Fig. 1 and the excitation and upconversion transitions involved in this work are indicated.

Figure 2 shows a typical emission spectrum of $^4D_{3/2}\rightarrow^4I_J$ transitions recorded for a sample with 1 at. % Nd^{3+}. An intense emission has been observed for the $^4D_{3/2}\rightarrow^4I_{11/2}$ transition located between 380 and 390 nm along with two groups of emission lines situated at around 353 and 415 nm corresponding to $^4D_{3/2}\rightarrow^4I_{9/2}$ and $^4D_{3/2}\rightarrow^4I_{13/2}$ transitions, respectively.

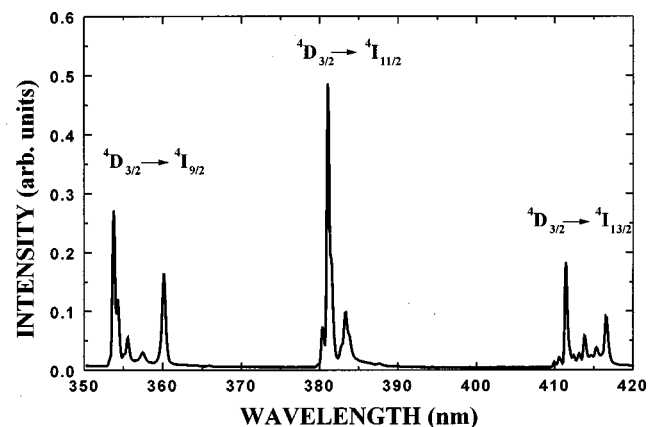FIG. 2. $^4D_{3/2}\rightarrow^4I_J$ upconversion spectrum for the 1 at. % Nd^{3+}-doped LaF_3 layer grown on CaF_2(111) substrate recorded at 25 K.
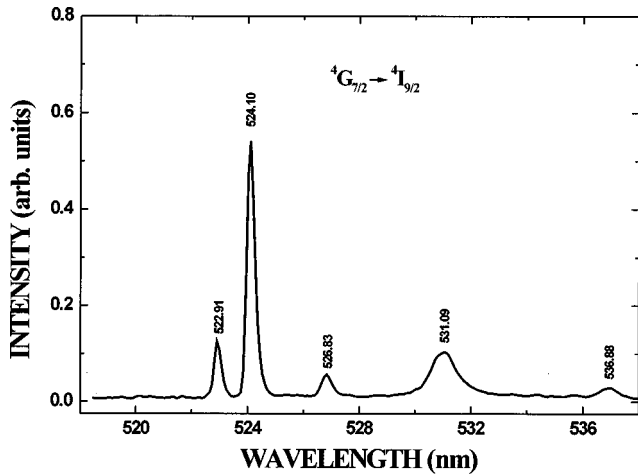
FIG. 3. Green upconversion from $^4G_{7/2} \rightarrow {}^4I_{9/2}$ transition for the same layer as Fig. 2 at 25 K.

The other two upconversion spectra are depicted in Figs. 3 and 4 for the same sample. The spectrum in Fig. 3 is ascribed to the transition of $^4G_{7/2} \rightarrow {}^4I_{9/2}$. Figure 4 shows that a couple of transitions are responsible for the upconversion emission observed between 570 and 600 nm. The emission lines resulting from the $^2G_{7/2} + {}^4G_{5/2} \rightarrow {}^4I_{9/2}$ transition are marked by a circle, whereas those corresponding to $^4G_{7/2} \rightarrow {}^4I_{11/2}$ transition are labeled by an asterisk. The remaining two lines marked with a plus are not clearly identified, and are probably due to the transition $^4D_{3/2} \rightarrow {}^4F_{3/2}$.

Excitation spectra for the upconversion emissions were obtained in two spectral ranges corresponding to the $^4I_{9/2} \rightarrow {}^4F_{5/2}$, $^2H_{9/2}$, and $^4I_{9/2} \rightarrow {}^4F_{3/2}$ transitions by monitoring the $^4D_{3/2} \rightarrow {}^4I_{11/2}$ transition at 381 nm and the $^4G_{7/2} \rightarrow {}^4I_{9/2}$ transition at 524 nm for the sample doped with 1 at. % Nd (Fig. 5). Some differences can be identified between the excitation spectra for uv and green or orange upconversions. For comparison purposes, the excitation spectrum recorded for infrared emission at 901 nm of the $^4F_{3/2} \rightarrow {}^4I_{9/2}$ transition is also shown in Fig. 5. Several excitation lines observed for infrared emission disappear from the spectra for upconversion emissions, especially for that obtained by monitoring the 381-nm emission line. This indicates that not all the ab-
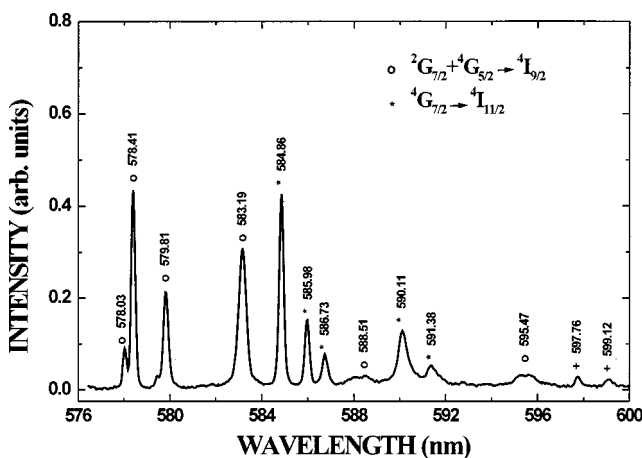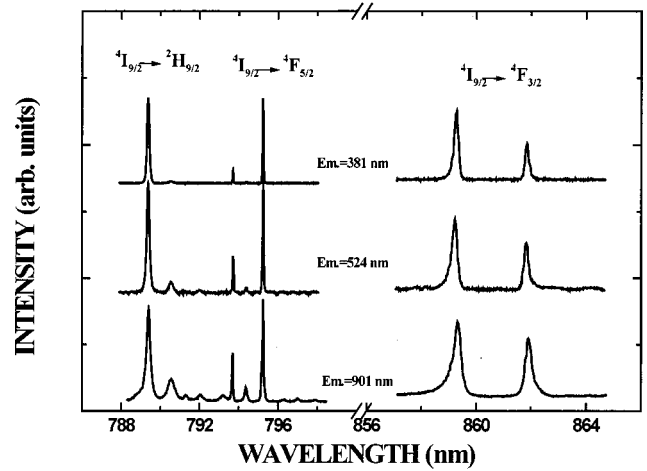

FIG. 5. Excitation spectra obtained by monitoring 381- and 524-nm upconversion lines as well as 901-nm infrared emission lines (from $^4F_{3/2} \rightarrow {}^4I_{11/2}$ transition) for the LaF$_3$:1 at. % Nd^{3+}/CaF$_2$(111) sample at 25 K.

sorption lines of Nd^{3+} could efficiently excite the upconversion emissions. Furthermore, a narrowing of the excitation linewidth has been detected at the two excitation regions. For example, the half-widths of the excitation lines are 0.12, 0.15 and 0.25 nm for the peak at 789.3 nm, and 0.25, 0.36, and 0.5 nm for that at 859.3 nm with monitoring the emissions at 381, 524, and 901 nm, respectively. This means that there is a selection of excitation wavelengths for these upconversion mechanisms. On the other hand, no excitation line corresponding to any excited-state absorption can be identified. This result rules out the possibility of the successive absorption process for the upconversion mechanisms.

In order to investigate the concentration dependence for the upconversion luminescence, a series of crystalline layers have been grown with Nd^{3+} concentrations ranging from 0.5 to 5 at. %. Figure 6 illustrates the results on the five upconversion emissions. For all samples, the uv upconversion at 381 nm corresponding to the $^4D_{3/2} \rightarrow {}^4I_{11/2}$ transition shows the most intense upconversion emission. As will be discussed later, this transition is due to a three-photon process.

FIG. 4. Orange upconversion from $^4G_{7/2} \rightarrow {}^4I_{11/2}$ and $^2G_{7/2} + {}^4G_{5/2} \rightarrow {}^4I_{9/2}$ transitions for the same layer Fig. 2 at 25 K.
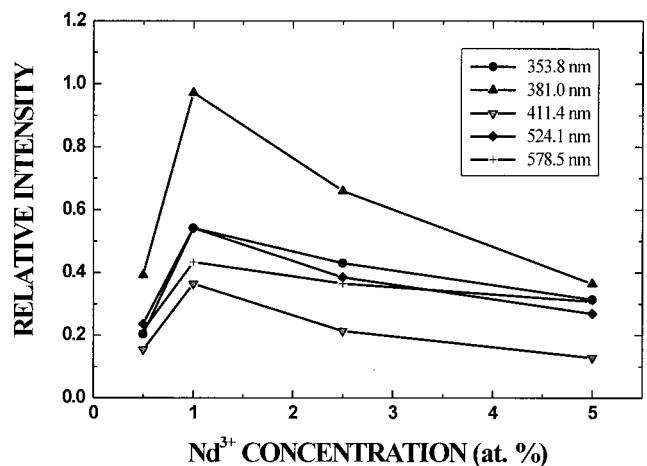

FIG. 6. Emission intensities for various upconversion lines from different transitions as a function of Nd^{3+} concentrations.
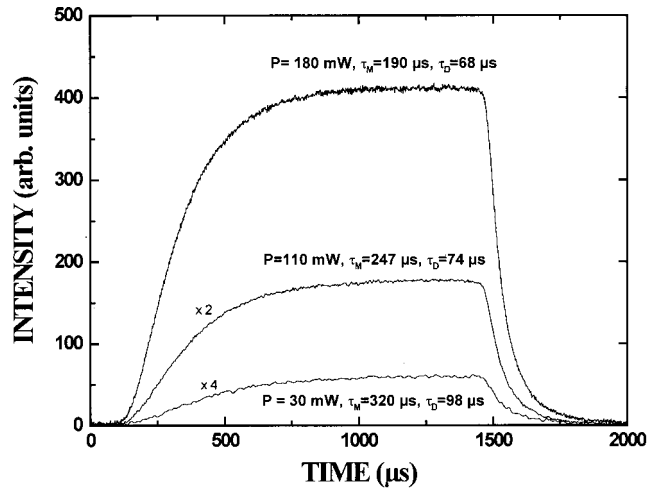
FIG. 7. Fluorescence rise and decay curves for the uv emission at 381 nm of 1 at. % Nd^{3+}-doped LaF_3 as a function of excitation power at 25 K.
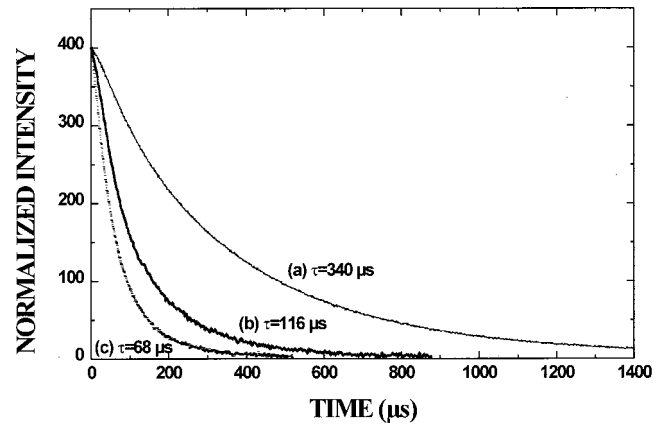

FIG. 8. Fluorescence decay curves for different emissions at 25 K of 1 at. % Nd^{3+}-doped LaF_3. (a) Infrared emission at 862 nm, (b) green emission at 524 nm, and (c) uv emission at 381 nm.

For all the transitions studied, the maximum of luminescence intensity is observed for a Nd^{3+} concentration of 1 at. % (nominal concentration), the same as that for the infrared emissions.[26,27]

B. Dynamic properties

The fluorescence rise and decay curves for the upconversion emissions and the infrared emission of the $^4F_{3/2} \rightarrow ^4I_{9/2}$ transition were measured with a digital oscilloscope. For all three upconversion emissions, the rise times are very similar. For example, at 25 K, for the 1 at. % Nd^{3+}-doped sample with 160-mW laser excitation, we have the values of 190 ± 10, 192 ± 10, and $200 \pm 10\,\mu s$ for 381-, 524-, and 578-nm emissions, respectively, while that for the infrared emission is about 360 μm. The rise times were obtained by fitting the experimental data with an exponential curve for the long time tail about 100 μs after cutoff of the excitation light. At low power excitation, the rise time is much longer than the one observed at high power excitation. With 789.3-nm excitation, the evolution of the fluorescence rise curve for the blue emission at 381 nm as a function of laser power is shown in Fig. 7.

For the decay curves, the decay times for green and orange upconversion emissions are very close to each other, while that for the blue emission is much shorter. The measured results are given in Table I. Just like for the rise-time measurement, we also reject the first part of the decay data to fit the decay times. The decay curves for different emissions are shown in Fig. 8.

C. Room-temperature upconversion in a guided configuration

The refractive indices obtained by using the m-lines method are 1.602 and 1.595 for ordinary and extraordinary indices of LaF_3 crystalline layers at 633 nm, while that for the CaF_2 substrate is 1.433. The large difference between the refractive indices of the LaF_3 layer and the CaF_2 substrate lead to a big numerical aperture for the Nd:LaF_3 planar waveguide (0.7), which facilitates the coupling of laser light into the planar waveguide. With a thickness of 3.6 μm, the

Nd:LaF_3 waveguides are multimodes, and a total number of seven modes has been detected for the emission and excitation wavelength studied.

The RT upconversion spectra were obtained in the guided configuration for the blue, green, and orange regions by using the prism-coupling method, and the spectra are given in Fig. 9 with 100 mW of pump power. Under nonguided excitation, the upconversion fluorescence of Nd^{3+} is quenched gradually with increasing temperature, and the spectrum disappears completely at about 100 K for a laser power of 100 mW. When the excitation light is guided into the layers, however, intense upconversion fluorescence that was very shiny to the human eye was observed with the same excitation power at RT. In addition, a new upconversion band located between 475 and 495 nm corresponding to the $^2K_{5/2} + ^2G_{9/2} \rightarrow ^4I_{9/2}$ transitions was observed. This transition is seldom detected in nonguided excitation in fluoride crystals, even at low temperature and for ordinary luminescence condition. Unlike the situation at low temperature, no three-photon upconversion emission was detected from the $^4D_{3/2}$ level at RT.
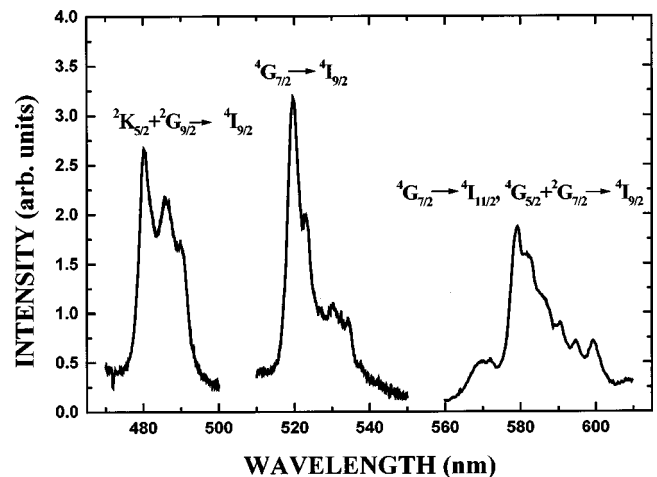

FIG. 9. Room-temperature guided upconversion emissions obtained for the 1 at. % Nd^{3+}-doped LaF_3 layer using the prism-coupling method with excitation at 787.7 nm.
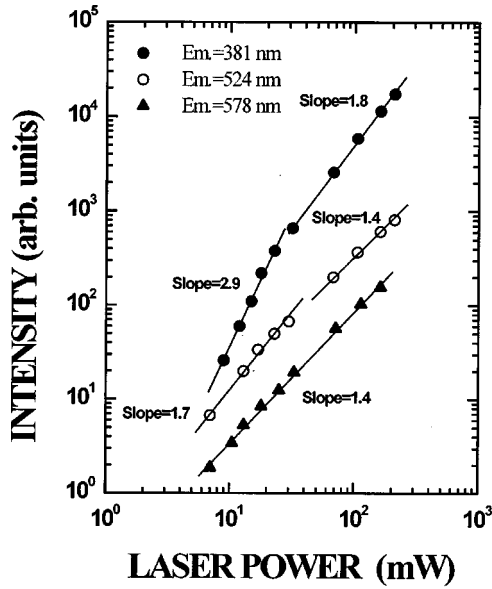
FIG. 10. Log-log plots for different upconversion emissions as a function of incident laser powers for LaF$_3$:1 at. % Nd^{3+}/CaF$_2$(111) at 25 K.

IV. DISCUSSION

A. Interpretation of the upconversion mechanisms

In a recent work on Nd^{3+}-doped fluoroindate glass, Menezes *et al.* have observed a weak uv upconversion at 382 nm due to a three-photon process with excitation into the $^4F_{3/2}$ level, which is 40 times smaller than the green emission at 522 nm.[18] The three-photon upconversion process was assigned to a three-body cooperative energy transfer where two excited Nd^{3+} ions in the $^4F_{3/2}$ level transfer their energy simultaneously to a third one excited in the same level. It is well known that the cooperative energy-transfer probability is very low compared to that of the successive energy transfer or sequential absorption processes. For our thin film samples, the uv upconversion is even more intense than the green and orange emissions at low temperature. Therefore, the proposed cooperative energy-transfer mechanism cannot be used to interpret our experimental results.

As mentioned above, three excited levels $^4D_{3/2}$, $^4G_{7/2}$, and $^2G_{7/2}+^4G_{5/2}$ are responsible for the observed upconversion fluorescence at low temperature. In order to investigate the excitation mechanisms for populating different emitting levels, the evolution of emission intensities corresponding to different transitions has been studied as a function of excitation power. This experiment gives evidence for the number of photons involved in the upconversion processes, which corresponds to the slope value of the fitted straight line in the log-log plot. The results shown in Fig. 10 are obtained by monitoring the relative intensities of the most intense peaks arising from each transition: the 381-nm line from the $^4D_{3/2}\rightarrow^4I_{11/2}$ transition, the 524-nm line from the $^4G_{7/2}\rightarrow^4I_{9/2}$ transition, and the 578-nm line from the $^2G_{7/2}+^4G_{5/2}\rightarrow^4I_{9/2}$ transition. According to the slopes of the fitted straight lines in the log-log plot, a three-photon upconversion process is assigned to the uv emission from the $^4D_{3/2}$ level (with a slope of 2.9), while a two-photon process is responsible for the green and orange upconversions from
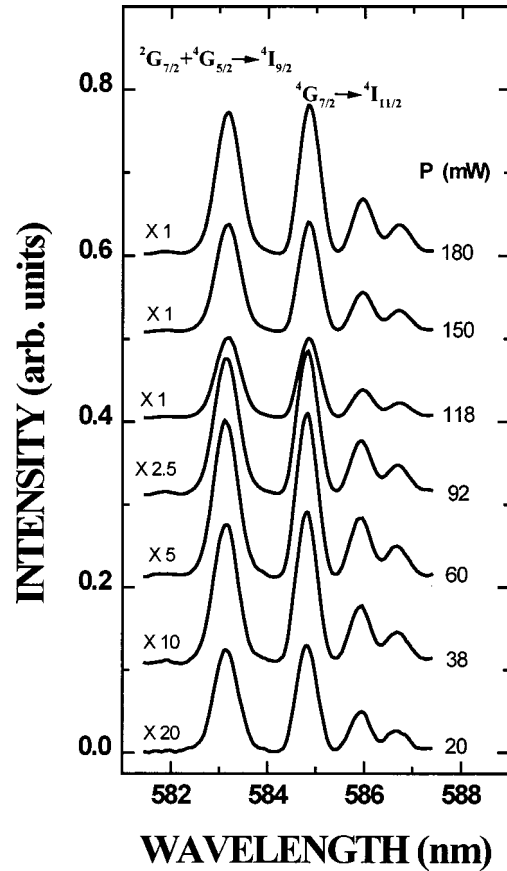

FIG. 11. Part of the emission spectra from $^4G_{7/2}\rightarrow^4I_{11/2}$ and $^2G_{7/2}+^4G_{5/2}\rightarrow^4I_{9/2}$ transitions measured at different excitation powers showing the emission intensity ratios between the two transitions with excitation at 789.3 nm.

$^4G_{7/2}$ and $^2G_{7/2}+^4G_{5/2}$ levels (slopes equal to 1.7 and 1.4, respectively). It can be seen that under high power excitation, a phenomenon of excitation saturation occurs especially for the uv and green emissions, which lead to a gradual decrease of the slopes for the dependent curves. Pollnau *et al.* have studied this phenomenon in different conditions.[4] They showed that almost in all upconversion systems the excitation saturation takes place under high excitation density resulting from the depletion of the intermediate excited states.[4]

The relative intensities of the two-photon upconversion emissions versus excitation powers can be investigated simultaneously by recording the emission spectra at 570–600 nm at different excitation powers. The results in Fig. 11 indicate that the intensity ratio for 583-nm emission from the $^2G_{7/2}+^4G_{5/2}\rightarrow^4I_{9/2}$ transition to 585-nm emission from the $^4G_{7/2}\rightarrow^4I_{11/2}$ transition remains practically unchanged with the 789-nm excitation. This evidence implies that the same pumping mechanism could probably populate the two emission levels, with an addition multiphonon process from the $^4G_{7/2}$ level to populate the $^2G_{7/2}+^4G_{5/2}$ level.

It is well established that the dynamic characteristics for upconversion processes constitute a useful tool in determining the corresponding excitation processes. From the results presented in Sec. IV B, we know that the rise times for the three upconversion emissions are very similar. This indicates that the predominant process for the three types of upconversion is the same and the intermediate level is $^4F_{3/2}$ for all cases.

TABLE I. Fluorescence decay times (μs) for upconversion emissions originating from different energy levels with 160-mW laser excitation at 789 nm.

	Nd^{3+} concentrations (at. %)			
Transitions	0.5	1.0	2.5	5.0
$^4D_{3/2} \rightarrow {}^4I_{11/2}$	88	68	41	25
$^4G_{7/2} \rightarrow {}^4I_{9/2}$	142	116	61	33
$^2G_{7/2} + {}^4G_{5/2} \rightarrow {}^4I_{9/2}$	152	118	63	34

The luminescence lifetimes of several excited levels of Nd^{3+} have been studied for 1% Nd^{3+}-doped LaF$_3$ bulk crystal at 77 K by Basiev *et al.*[28] and decay times for the three levels studied in this work are 35 μs, 110.5 ns, and 29.2 ns corresponding to $^4D_{3/2}$, $^4G_{7/2}$, and $^2G_{7/2} + {}^4G_{5/2}$ levels, respectively. In the epitaxial layers, the intrinsic decay times should be in the same range as those obtained in bulk crystals, just as being observed for the infrared emissions.[26,27] Compared with the values given in Table I, it is obvious that all the decay times observed for the $^4G_{7/2}$, $^2G_{7/2} + {}^4G_{5/2}$, and $^4D_{3/2}$ levels have no close relation with their intrinsic lifetimes. Therefore, the successive absorption process cannot be the predominant process since in that case the measured decay time corresponds to the intrinsic lifetime of the level. The main upconversion mechanisms should be due to some kinds of energy transfer and/or energy cross relaxation between different Nd^{3+} ions.

From the energy levels of Nd^{3+} in LaF$_3$ crystals reported by Caspers[29] and Vignaneswara,[30] there exist two possible resonant energy-transfer processes in populating the green and orange upconversion upper levels and one transition in populating the uv upconversion level. After the ground-state absorption for the first step to excite the $^4F_{3/2}$ level, these possible cross-relaxation energy transfers are as follows (the capital letters are used to label the levels for simplifying the discussion below):

$$^4I_{9/2} + h\upsilon \rightarrow {}^4F_{3/2}(X), \tag{1}$$

$$^4F_{3/2}(X) + {}^4F_{3/2}(X) \rightarrow {}^4I_{11/2}(Z) + ({}^2K_{15/2} + {}^2G_{9/2})(A), \tag{2}$$

$$^4F_{3/2}(X) + {}^4F_{3/2}(X) \rightarrow {}^4I_{13/2}(Y) + {}^4G_{7/2}(B), \tag{2'}$$

$$^4F_{3/2}(X) + {}^4G_{7/2}(B) \rightarrow {}^4I_{11/2}(Z) + {}^2L_{15/2}(C). \tag{3}$$

Considering that only the lowest Stark level for the initial states could be populated at very low temperature, some possible energy combinations for the above-mentioned energy-transfer processes are given in Table II. The energy mismatches given in Table II indicate that some resonant or quasiresonant energy transfers are found for all the three processes.

Therefore, the upconversion mechanism in this system can be described as follows: in the first step, the pump laser excites Nd^{3+} from the ground state to the $^4F_{3/2}$ or $^2H_{9/2} + {}^4F_{5/2}$ levels depending on the pump wavelength selected arround 859 or 789 nm, respectively. In the latter case, the excited Nd^{3+} ions decay to the $^4F_{3/2}$ level by fast multiphonon relaxation immediately after excitation. Second,

TABLE II. Some ion-pair energy combinations for the energy-transfer processes.

Initial levels (cm^{-1})	Final levels (cm^{-1})	ΔE (cm^{-1})
$X(11595) + X(11595)$	$Z(1980) + A(21201)$	$+9$
$X(11595) + X(11595)$	$Z(1980) + A(21234)$	-24
$X(11595) + X(11595)$	$Z(1980) + A(21254)$	-44
$X(11595) + X(11595)$	$Z(2038) + A(21158)$	-6
$X(11595) + X(11595)$	$Z(2038) + A(21176)$	-24
$X(11595) + X(11595)$	$Z(2069) + A(21158)$	-37
$X(11595) + X(11595)$	$Y(3919) + B(19251)$	$+20$
$X(11595) + X(11595)$	$Y(3919) + B(19235)$	$+36$
$X(11595) + X(11595)$	$Y(3974) + B(19235)$	-19
$X(11595) + X(11595)$	$Y(3974) + B(19251)$	-45
$X(11595) + X(11595)$	$Y(4038) + B(19147)$	$+5$
$X(11595) + X(11595)$	$Z(4077) + B(19147)$	-34
$X(11595) + B(19147)$	$Z(1980) + C(28823)$	-61
$X(11595) + B(19147)$	$Z(2188) + C(28544)$	$+10$
$X(11595) + B(19147)$	$Z(2188) + C(28525)$	$+29$
$X(11595) + B(19147)$	$Z(2223) + C(28525)$	-6
$X(11595) + B(19147)$	$Z(2223) + C(28544)$	-25

two adjacent excited Nd^{3+} ions in the $^4F_{3/2}$ state interact with each other inducing two energy-transfer processes (2) and (2'). As a result, one ion reexcites to a higher-energy level ($^2K_{5/2} + {}^2G_{9/2}$ or $^4G_{7/2}$) and the other deexcites to the ground state from the $^4I_{11/2}$ or $^4I_{13/2}$ levels by radiative or nonradiative processes.

The $^4G_{7/2}$ and $^2G_{7/2} + {}^4G_{5/2}$ states are therefore populated by these processes and by fast multiphonon processes from the upper-lying levels. In a third step, an addition cross-relaxation process involving two Nd^{3+} ions excited in $^4F_{3/2}$ and in $^4G_{7/2}$ states excites one ion to the upper $^2L_{15/2}$ state and the other returns to the $^4I_{11/2}$ level (3). According to the results in Table II, this third step is also resonant. Thus, on the populated $^4G_{7/2}$ level, there exists a competition among the energy cross relaxation to the upper level, a radiative transition to the ground state, and nonradiative decay to the $^2G_{7/2} + {}^4G_{5/2}$ levels. Since the third energy transfer is resonant, it could be very efficient. This is probably the reason for the observation mentioned above that the three-photon upconversion is even more efficient than the two-photon green and orange emissions. The proposed upconversion process is shown in Fig. 12 and will be confirmed in the following section by a rate-equation analysis. We will see that the analytical results are quite supportive for the proposed energy-transfer processes.

B. Rate-equation analysis

In order to verify the proposed upconversion mechanisms, we deal with the rate equations in this section for the processes described in Fig. 12. To simplify the system, we define all the ^4I_J states as level 1, $^4F_{3/2}$, $^4F_{5/2}$, $^2H_{11/2}$ manifolds as level 2, all the excited levels involved in the second step ($^4G_{7/2}$, $^4G_{5/2}$, $^2G_{7/2}$) as level 3, and the $^4D_{3/2}$ level as level 4. Let N_i, W_i, and τ_i represent the population, the radiative and nonradiative decay rate, and the lifetime from
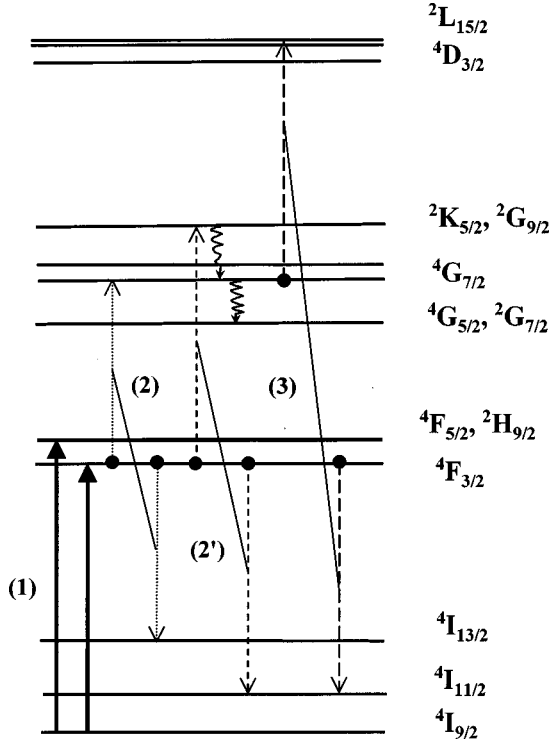
FIG. 12. Energy-level diagram for the proposed upconversion mechanisms.

level i, respectively, ρ is the pump rate from level 1, and finally C_i is the energy-transfer rate of the three processes. Then, the rate equations for the three excited levels of the four-level system can be written as follows:

$$\frac{dN_2}{dt} = \rho N_1 - W_2 N_2 - 2(C_1 + C_2)N_2^2, \qquad (4)$$

$$\frac{dN_3}{dt} = -C_3 N_2 N_3 - W_3 N_3 + (C_1 + C_2)N_2^2, \qquad (5)$$

$$\frac{dN_4}{dt} = C_3 N_2 N_3 - W_4 N_4. \qquad (6)$$

We consider now the decay characteristics of the excited levels. When the light is cut off, $\rho = 0$. Letting $C = C_1 + C_2$, we have

$$\frac{dN_2}{dt} = -W_2 N_2 - 2C N_2^2, \qquad (7)$$

$$\frac{dN_3}{dt} = -C_3 N_2 N_3 - W_3 N_3 + C N_2^2, \qquad (8)$$

$$\frac{dN_4}{dt} = C_3 N_2 N_3 - W_4 N_4. \qquad (9)$$

Under a weak excitation condition, the population of level 2 is not very high, and it is reasonable to consider

$$W_2 N_2 \gg 2C N_2^2.$$

Further simplification can be taken by considering $W_3 N_3 \gg C_3 N_2 N_3$ for very low power excitation. Therefore, the above equations can be solved, and the following equations can be obtained by taking $\tau_i = 1/W_i$:

$$N_2(t) = N_2(0)\exp\left(-\frac{t}{\tau_2}\right), \qquad (10)$$

$$N_3(t) = A_1 \exp\left(-\frac{t}{\tau_3}\right) + A_2 \exp\left(-\frac{2t}{\tau_2}\right), \qquad (11)$$

$$N_4(t) = B_1 \exp\left(-\frac{(\tau_2 + \tau_3)t}{\tau_2 \tau_3}\right) + B_2 \exp\left(-\frac{3t}{\tau_2}\right)$$
$$+ B_3 \exp\left(-\frac{t}{\tau_4}\right), \qquad (12)$$

where A_i and B_i are constants:

$$A_1 = N_3(0) - \frac{C\tau_2\tau_3}{\tau_2 - 2\tau_3}N_2^2(0), \quad A_2 = \frac{C\tau_2\tau_3}{\tau_2 - 2\tau_3}N_2^2(0),$$

$$B_1 = \frac{C_3 N_2(0)\tau_2\tau_3\tau_4}{\tau_2\tau_3 - \tau_3\tau_4 - \tau_2\tau_4}A_1, \quad B_2 = \frac{C_3 N_2(0)\tau_2\tau_4}{\tau_2 - 3\tau_4}A_2,$$

$$B_3 = N_4(0) - (B_1 + B_2),$$

and $N_i(0)$ is the initial population of level i at $t = 0$.

From Eq. (10) we find that with a reasonable simplification, the decay of levels 2 is exponential, and the decay time is characterized by the intrinsic lifetimes of this level. This result coincides with the experimental decay time obtained by fitting the experimental data with rejecting the first 100 μs in the decay curve. We have also measured the decay characteristics of the $^4F_{3/2}$ level with different excitation wavelengths, both the upconversion excitation line (such as the 789.3-nm excitation line in Fig. 5) and the nonupconversion ones (such as the line at 790.6 nm); no difference can be identified for the decay curve as well as the time constant. With 120-mW laser excitation, the decay time is about 340 μm for both excitations. This means that the upconversion process has induced no significant influences on the $^4F_{3/2}$ level lifetime.

However, Eqs. (11) and (12) have revealed some interesting features for the decay characters of the relevant levels. For level 3, the decay curve is composed of two features: one corresponds to a decay time constant of τ_3 and the other is related to $\tau_2/2$, while for level 4, three time constants are involved in the decay curves, which are corresponding to τ_4, $1/(1/\tau_3 + 1/\tau_2)$, and $\tau_2/3$, respectively. Taking into account of the intrinsic lifetimes of the levels involved in the upconversion processes, Eqs. (11) and (12) can be simplified. Since τ_3 is very small compared to τ_2, the decay curve of the level 3 is only predominated by the second term in Eq. (11). The time constant for the first term in Eq. (12) becomes τ_3, which can also be neglected. We can therefore rewrite the two equations as follows:

$$N_3(t) = A_2 \exp\left(-\frac{2t}{\tau_2}\right), \qquad (13)$$

$$N_4(t) = B_2 \exp\left(-\frac{3t}{\tau_2}\right) + B_3 \exp\left(-\frac{t}{\tau_4}\right). \qquad (14)$$

Equations (13) and (14) demonstrate that the decay of the two-photon process goes as $\tau_2/2$, whereas that of the three-photon upconversion is characterized by two time constants τ_4 and $\tau_2/3$. Note that the obtained values in Table I for the green and orange upconversions are not exactly corresponding to the half of the lifetime of level 2 ($^4F_{3/2}$). Two reasons could be responsible for this difference. In the first place, the results given in Table I were obtained with a relatively high excitation power (160 mW), and under low power excitation the decay time is much longer, as shown in Fig. 7. The second reason is that some simplifications have been taken in the above treatment for the rate equations. Especially, we have neglected the $C_3N_2N_3$ term in the treatment above, which could lead to an extra decay time shortening for the level 3. The same reason can be used to explain the differences between the experimental results and the predicted value from the rate-equation analysis for level 4. Therefore, the obtained results show us the tendency of the evolution of the decay characters for the upconversion fluorescence.

We have shown that at RT and with guided configuration no three-photon upconversion was observed. A possible reason is that the intrinsic lifetime of the $^4G_{7/2}$ level is too short to allow an energy relaxation involving this level. On the other hand, the observation of the blue upconversion from the $^2K_{5/2} + {}^2G_{9/2}$ levels at the RT guided configuration is owing to the very high excitation density under the guided condition.

V. CONCLUSION

Room-temperature guided upconversion emissions at blue, green, and orange spectral regions were observed in Nd^{3+}-doped LaF_3 planar waveguides elaborated on (111) oriented CaF_2 substrates upon excitation in the near-infrared region by a Ti:sapphire laser. An efficient uv, green, and orange upconversion luminescence has been demonstrated and discussed at low temperature about 25 K. The uv blue emission originating from Nd^{3+} $^4D_{3/2} \rightarrow {}^4I_J$ ($J = \frac{9}{2}$, $\frac{11}{2}$, and $\frac{13}{2}$) transitions is the most efficient upconversion fluorescence observed in spite of its three-photon upconversion character. Other upconversion emissions in the green and orange regions are ascribed to the $^4G_{7/2} \rightarrow {}^4I_{9/2}$, $^2G_{7/2} + {}^4G_{5/2} \rightarrow {}^4I_{9/2}$, and $^4G_{7/2} \rightarrow {}^4I_{11/2}$ transitions, respectively.

Upconversion mechanisms have been proposed for different upconverted emissions by analyzing the fluorescence dynamic properties (fluorescence rise and decay curves) and the evolution of emission intensities with incident laser power. The cross-relaxation energy-transfer processes involving two Nd^{3+} ions excited in the $^4F_{3/2}$ state are suggested for the green and orange upconversions. For uv blue upconversion, a third cross-relaxation energy transfer involving two Nd^{3+} ions excited in different states as $^4F_{3/2}$ and $^4G_{7/2}$ to produce the population of the $^4D_{3/2}$ level. A rate-equation analysis is then applied to this system, and the results are quite supportive for the proposed mechanisms. The concentration dependence study has shown that the optimum concentration for the Nd^{3+} dopant is about 1 at. % for these epitaxial layers for all the upconversion emissions observed.

The efficient room-temperature guide upconversion observed in the Nd^{3+}-doped LaF_3 waveguide suggests that this kind of thin film waveguide could be a prospective source to obtain RT upconversion lasers.

*Corresponding author. Email address: exzhang@ntu.edu.sg. Also with the Laboratory of Excited State Processes, Chinese Academy of Sciences, 130021 Changchun, P. R. China.

[1] W. Lenth and R. Macfarlane, Opt. Photonics News **March**, 8 (1992).

[2] N. Pelletier-Allard and R. Pelletier, Phys. Rev. B **36**, 4425 (1987).

[3] M. F. Joubert, S. Guy, and B. Jacquier, Phys. Rev. B **48**, 10 031 (1993).

[4] M. Pollnau, D. R. Gamelin, S. R. Lüthi, and H. U. Güdel, Phys. Rev. B **61**, 3337 (2000).

[5] K. W. Krämer, H. U. Güdel, A. V. Butashin, and A. A. Kaminskii, Phys. Rev. B **60**, 5312 (1999).

[6] M. F. Joubert, Opt. Mater. **11**, 181 (1999).

[7] A. A. Kaminskii, *Laser Crystals*, 2nd ed., Springer Series in Optical Sciences Vol. 14, edited by D. L. MacAdam (Springer-Verlag, Berlin, 1990).

[8] Y. Guyot, H. Manna, J. Y. Rivoire, R. Moncorgé, E. Garnier, E. Descroix, M. Bon, and P. Laporte, Phys. Rev. B **51**, 784 (1995).

[9] S. Guy, M. F. Joubert, and B. Jacquier, Phys. Rev. B **47**, 11 001 (1993).

[10] V. Ostroumov, T. Jensen, J.-P. Meyn, G. Huber, and M. A. Nogi-nov, J. Opt. Soc. Am. B **15**, 1052 (1998).

[11] B. R. Reddy and P. Venkateswarlu, J. Chem. Phys. **79**, 5845 (1983).

[12] R. Buisson, J. Q. Liu, and J. C. Vial, J. Phys. (Paris) **45**, 1533 (1984).

[13] S. Huang, S. T. Lai, L. Luo, W. Jia, and W. M. Yen, Phys. Rev. B **24**, 59 (1981).

[14] R. M. McFarlane, F. Fong, A. J. Silversmith, and W. Lenth, Appl. Phys. Lett. **52**, 1300 (1988).

[15] W. Lenth and R. M. McFarlane, J. Lumin. **45**, 346 (1994).

[16] D. S. Funk, J. W. Carlson, and J. G. Eden, Electron. Lett. **30**, 1859 (1994).

[17] D. L. Russell, B. Henderson, B. C. Chai, J. F. H. Nicolls, and K. Holliday, Opt. Commun. **134**, 398 (1997).

[18] L. de S. Menezes, C. B. Araújo, G. S. Maciel, Y. Messaddeq, and M. A. Aegerter, Appl. Phys. Lett. **70**, 683 (1997).

[19] E. Daran, L. E. Bausá, R. Legros, C. Fontaine, and J. Garcia Solé, Solid State Commun. **94**, 379 (1993).

[20] M. Lui, R. A. Macfarlane, D. Yap, and D. Lederman, Electron. Lett. **29**, 172 (1993).

[21] S. Uda, K. Adachi, K. Inaba, T. Yao, A. Kasuya, and T. Fukuda, Jpn. J. Appl. Phys., Part 2 **36**, L41 (1997).

[22] R. A. Macfarlane and M. Lui, US Patent, No: 5,393,311 (1995).

[23] E. Daran, D. Shepherd, T. Bhutta, and C. Serrano, Electron. Lett. **35**, 398 (1999).

[24] E. Daran, R. Legros, A. Muñoz-Yagüe, C. Fontaine, and L. E. Bausá, J. Appl. Phys. **75**, 2749 (1994).

[25] W. T. Carnall, H. Crosswhite, and H. M. Crosswhite (unpublished); see also Ref. 12.

[26] X. Zhang, F. Lahoz, C. Serrano, G. Lacoste, and E. Daran, IEEE J. Quantum Electron. **36**, 243 (2000).

[27] F. Lahoz, E. Daran, X. Zhang, A. Muñoz-Yagüe, R. Cases, and R. Alcala, J. Appl. Phys. **86**, 3699 (1999).

[28] T. T. Basiev, A. Yu. Dergachev, Y. V. Orlovskii, and A. M. Prokhorov, J. Lumin. **53**, 19 (1992).

[29] H. H. Caspers, H. E. Rast, and R. A. Buchanan, J. Chem. Phys. **42**, 3214 (1965).

[30] U. Vignaneswara, K. H. Jagannath, D. R. Rao, and P. Venkateswarlu, Indian J. Phys. **50**, 90 (1976).